Quantization condition of quantum-well states in Cu/Co(001)

J. M. An,[1,*] D. Raczkowski,[2] Y. Z. Wu,[3,4] C. Y. Won,[3,4] L. W. Wang,[2] A. Canning,[2] M. A. Van Hove,[1,3,5] E. Rotenberg,[1] and Z. Q. Qiu[3,4]

[1]*Advanced Light Source, Lawrence Berkeley National Laboratory, Berkeley California 94720, USA*
[2]*Computational Research Division, Lawrence Berkeley National Laboratory, Berkeley California 94720, USA*
[3]*Materials Sciences Division, Lawrence Berkeley National Laboratory, Berkeley California 94720, USA*
[4]*Department of Physics, University of California, Berkeley, California 94720, USA*
[5]*Department of Physics, University of California, Davis, California 95616, USA*

(Received 10 April 2003; published 21 July 2003)

Recent photoemission data exhibit individual quantum-well states (QWSs) at integer numbers (1–20) of monolayers in a Cu(001) film grown on a Co(001) substrate film, itself grown pseudomorphically on Cu(001). *Ab initio* calculations confirm the concept of the quantization condition inherent in the phase accumulation model (PAM) to predict the energies of QWSs as a function of their thickness, and provide new insight into their nature. In addition, it is shown that band structures and reflection phases obtained from either experiment or ab initio theory can quantitatively predict QWS energies within the PAM model. It is shown that a simple superposition of oppositely traveling Bloch states, phase-shifted by the reflections from surface and interface, gives an excellent representation of the QWSs within the ultrathin film. We point out an improvement to the standard local density approximation to better represent the image potential of the free surface and its influence on QWS. It is also shown that QWSs are tolerant of interdiffusion across the Co/Cu interface, which may broaden the photoemission peaks characteristic of QWSs.

DOI: 10.1103/PhysRevB.68.045419 PACS number(s): 73.21.Fg, 79.60.Jv, 79.60.Dp, 73.22.Dj

I. INTRODUCTION

Metallic thin films display a variety of interesting properties associated with quantum-well states (QWSs). For example, the oscillatory magnetic interlayer coupling[1] was recently shown to result from the QWSs in the spacer layer.[2,3] QWSs from a capping layer was also found to modulate the magnetic anisotropy of a ferromagnetic thin film.[4] Furthermore, structural stability of Ag thin films grown on Fe(100) has been revealed by angle-resolved photoemission experiments to be directly related to the QWSs in the Ag layer.[5]

The above discoveries generated a widespread interest in the search for other properties associated with QWSs in metallic thin films. Theoretically, understanding the electronic structures of such metallic thin films can provide necessary guidance for designing new materials with predictable properties. Experimentally, recent advances in thin film synthesis and measurement techniques allow for a highly accurate experimental determination of the QWSs and their associated properties.

In this paper, we present recently measured angle-resolved photoemission (PE) intensity data that show individual QWSs at integer numbers of Cu monolayers in a wedged Cu thin film system deposited on a Co (001) substrate. The QWSs are revisited in the highly resolved energy window $E\text{-}E_F = 0 \sim -1.9$ eV of the PE data. The experimental electronic properties of the QWS are compared with our first principles simulations where we have corrected the bulk Cu band structure to the true band structure mapped by recent angle-resolved photoemission spectroscopy (ARPES) measurements.[6,7] It has been shown recently for bulk Cu that highly accurate PE data give significant deviations from density functional theory results for the occupied states.[6–9] Until now, no computational attempts have been made to correct the bulk band structure discrepancy between theory and experiment in the calculation of QWS energies. In general, the formation of the QWSs has been known to be caused by potential barriers. It is thus important to investigate the QWSs based on more accurate bulk electronic energies and relaxed equilibrium atomic positions at the surface and interface. Most of the calculations reported so far are based on Korringa-Kohn-Rostoker Green's function methods[10–12] using the local density approximation (LDA).[13,14] In this paper, using the plane wave norm-conserving pseudopotential method, we determine QWSs by analyzing the wave functions directly in real space.

Typically, the QWS energies are measured by PE as a function of Cu thickness, and are classified according to the number ν of nodes in the envelope electron wavefunctions following the phase accumulation model (PAM).[15] The modeled QWS energies are obtained via a nearly-free-electron dispersion relation $E(k_\perp)$ along the Γ-X line and the PAM surface and interface phase formulas.[15] Although the PAM successfully explains the evolution of the QWS in the energy-thickness plane, it is also noticed that the PAM results deviate from results of a more accurate tight-binding model.[15] In the PAM, the phase at the interface is calculated using a step-function energy barrier whose height equals the minority-spin energy band gap of the ferromagnetic substrate. This is obviously an oversimplified approximation, especially when the ferromagnetic band gap is a hybridized gap such as in the Co case and when the interlayer mixing occurs where the use of the step-function energy barrier is less justified. Unfortunately, the QWS positions in the energy-thickness plane depends less sensitively on the value of the PAM phase, making it difficult to examine the validity of the PAM. As shall be reported in this paper, the accurate experimental data from our recent measurement allow us to

examine the PAM phase. It turns out that the PAM phase is different from the experimentally and calculated total phases, although it is conceptually correct and gives reasonably good QWS energies as a function of film thickness.

II. EXPERIMENT

A Cu(001) single crystal was prepared by mechanical polishing down to 0.25-μm diamond paste followed by electrochemical polishing.[16] Then the Cu substrate was cleaned *in situ* with cycles of Ar ion sputtering at 1.5 keV and annealing at 600–700 °C until sharp low energy electron diffraction diffraction spots were observed. An 8-ML Co film was grown pseudomorphically on Cu(001) to serve as the ferromagnetic substrate; the Co film has a structure close to fcc. Then a Cu wedge with a slope of ~ 5 ML/mm was grown on top of the Co for the QWS study. Both the Co and Cu films were grown at room temperature, and their growth rate was measured by a quartz crystal oscillator. The base pressure was $\sim 3\times 10^{-10}$ torr, and the pressure during the growth was $\sim 1.4\times 10^{-9}$ torr.

X-ray photoemission measurement was performed at beamline 7.0.1.2 of the Advanced Light Source at the Lawrence Berkeley National Laboratory. The small beam size ($\sim$50-100 μm) gave a thickness resolution $\sim$0.3–0.5 ML on the wedged sample. An 83-eV photon energy was used to select the electronic states near the belly of the Cu Fermi surface. The photoemission electrons in the normal direction were collected by a Scienta SES-100 analyzer which simultaneously measures the energy and angular spectra. The angular window for the photoemission spectra is $\sim 1°$. QWSs associated with discrete Cu layers can be clearly observed, showing a layer-by-layer growth manner of the Cu film on Co(001). The Cu thickness can be accurately determined by assigning those discrete QWS to integer number of Cu layers. The result is consistent with the value measured by the quartz crystal oscillator. Moreover, this method also determines the starting point of the Cu wedge precisely which is always difficult to determine accurately using other methods (such as using the Cu 3*p* core level intensity).

III. COMPUTATIONAL METHOD

The calculations presented here are based on density functional theory (DFT) (Refs. 13,14, and 17) and the Perdew-Burke-Ernzerhof Generalized Gradient Approximation (PBE-GGA) (Refs. 18 and 19) to the exchange-correlation functional, as implemented in the norm-conserving pseudopotential plane-wave parallel codes PARATEC and PETOT.[20] Pseudopotentials of the Hammann and Troullier-Martins type[21–23] were generated with the FHI98PP pseudopotential program. The 3*s*, 3*p*, and 3*d* states are included for the Cu and Co valence electrons. For the (001)-oriented thin film, we have used $(a/2,a/2,0)$ and $(a/2,-a/2,0)$ as the unit cell periodicity in the lateral directions, where *a* is the bulk Cu lattice constant. Given such a unit cell, we have used a $8\times 8\times 2k$-point grid for *k*-space integration. Correspondingly, we have used a cold smearing method[24] for Fermi surface smearing. This method allows us to use a 0.1-eV smearing energy without causing significant errors in the Fermi energy. A kinetic energy cutoff of 60 Ry was used to expand the electronic wavefunctions in the plane-wave basis.

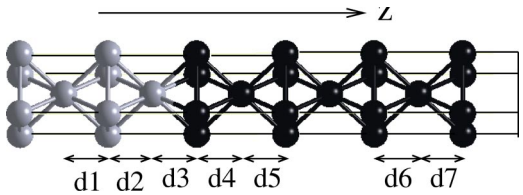

FIG. 1. The film structure of Co_4/Cu_7 with free surface at right has the following optimized interlayer distances: d1 = 1.747 Å, d2 = 1.688 Å, d3 = 1.818 Å, d4 = 1.775 Å, d5 = 1.788 Å, d6 = 1.808 Å, and d7 = 1.789 Å; all the other spacings are 1.805 Å for Cu and 1.76 Å for Co. Cu atoms are denoted by black spheres and Co atoms are indicated by gray spheres, all of which are enclosed in the tetragonal supercell aligned in the surface normal direction (z).

In the absence of experimental structural information on the Cu surface and Cu/Co interface in this system, we have optimized the structure using a quasi-Newton method,[25] until the forces are decreased to within 0.004 Ry/a.u.. A few layers of surface and interface Cu and Co atoms are relaxed, while other Cu (Co) atoms are maintained at their bulk positions. The lateral lattice constant *a* is 3.61 Å, the bulk value of Cu, since in the experiment, the whole Cu/Co bilayer system is grown pseudomorphically on a bulk Cu substrate. Because of this, the interlayer distance in the center of the Cu film is 1.805 Å and in the ''bulk'' of the Co film 1.76 Å, as shown in Fig. 1. In all the calculations, 4 ML of Co are used to simulate the substrate Co layers. Test simulations with 4 to 7 ML of Co indicated no significant energy change in the QWS. All of our simulations were performed on IBM SP computers at the NERSC computing center.

IV. RESULTS AND DISCUSSION

A. Bulk band structure

Our calculated local density approximation (LDA) and the GGA band structures for bulk Cu were found to be almost identical and are shown in Fig. 2 as the dotted curves. They both deviate somewhat from the experimental results[26] due to a well-known DFT-LDA/GGA band structure error. There are two significant errors in the bulk band structure that would cause errors in QWS calculations. First, relative to the Fermi energy, the calculated *d*-state band is at least 0.5 eV too high. Second, the *sp*-state band along the Δ_1 direction, which is responsible for the formation of QWS in the Cu/Co (001) thin film, is about 0.3 eV too low. Compared to experiment the GGA/LDA calculation yields the *d*-like Δ_5 and Δ_2 bands too high at $E\text{-}E_F = -1.64$ eV and -1.73 eV for X_5 and X_2 states, respectively. As a result, this leads to the occurence of *d*-like QWS for emission energies larger than 1.6 eV, which was also the case in the calculation of Nordström *et al.*[10] However, in the experiment, only *sp*-like QWSs are seen up to emission energies of 2 eV. Recently the LDA/GGA error has been studied in more detail for bulk Cu, via a full three-dimensional mapping of crystal momentum wave vector **k** with ARPES experiments in conjunction with

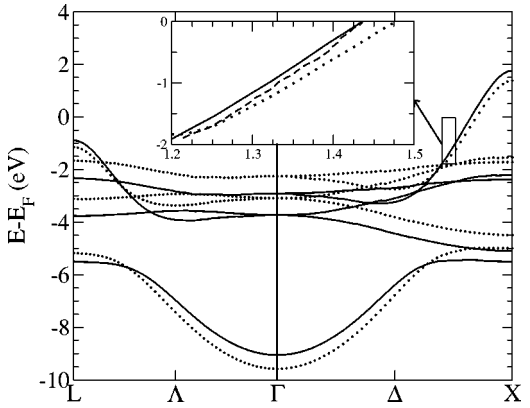

FIG. 2. The Cu band structures along the L-Γ-X line: GGA bands are denoted by dotted curves; corrected bands are indicated by solid curves. The inset zooms in on *sp*-like Δ_1 bands in the region $k_\perp = 1.2 \sim 1.5$ Å^{-1} along the Γ-X line, where the band determined by fitting the experimental QWS is denoted by a dashed curve.

full-potential DFT calculations.[6,7] It has been shown that the LDA/GGA Cu band energies are not only off by a few tenths of an eV, dependent on **k** and the band index, but also the relative band locations are misplaced.[6,7] This prompted a series of more accurate *ab initio* calculations within the *GW* approximation (GWA) for bulk Cu.[8,9] The *ab initio* GW calculations are strikingly similar to the measured Cu band structure showing the importance of the dynamic exchange-correlation potential or the self-energy in considering the excited states properties of even weakly-correlated metals such as Cu.

However, *GW* calculations can not be performed for our current layered structure due to the heavy computational cost. Instead, we have modified our LDA/GGA nonlocal pseudopotentials in order to fit the experimental bulk Cu band structure. We have added simple Gaussian terms in the *s*, *p*, and *d* nonlocal pseudopotentials of Cu, and fitted the bulk band structure at several symmetry points: L-Γ-X. A more detailed description of this fitting procedure is given in Ref. 27. The resulting fitted bulk Cu band structure is shown in Fig. 2 as the solid curves.

B. Quantum-well states

We used the fitted Cu pseudopotential to perform *ab initio* calculations for the Cu/Co (001) systems with 4 ML of Co and up to 17 ML of Cu. Then we compared our calculated results with previously reported DFT/LDA calculations and our high resolution experimental PE data. Unlike the aforementioned Korringa-Kohn-Rostoker Green's function calculations,[10–12] our pseudopotential calculation allows us to directly associate the QWS with the electron wave functions. To this end, we take the average of the wave function squared over the lateral plane and plot the results in the *z* direction. We then identify QWS according to the envelope nodal structures. In Fig. 3, the lateral averaged wavefunction squared shows an envelope nodal structure that modulates faster atomic scale oscillations.

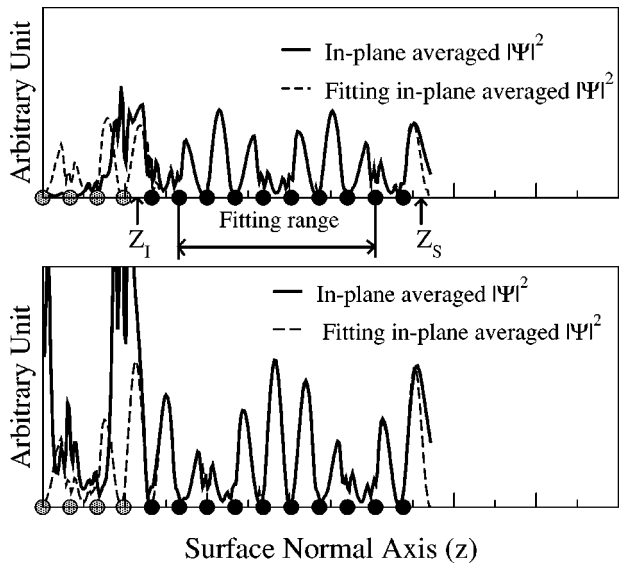

FIG. 3. Calculated in-plane average electron charge densities $|\Psi(z)|^2$ for the Co_4/Cu_{10} system are shown with respect to the fitting standing waves expressed in Eq. (4): (top panel) $E-E_F = -1.3$ eV corresponding to $\nu = 3$; (bottom panel) $E-E_F = -0.28$ eV corresponding to $\nu = 2$. The overlap magnitudes between the fitting (dashed) and the calculated (solid) charge densities for both QWSs reach 99% in the indicated fitting range. The underlying Cu (Co) atoms are depicted by black (gray) circles.

Our calculated minority-spin QWS energy levels at the surface Brillouin zone center $\bar{\Gamma}$ (corresponding to the normal photoemission direction in the experiment) are shown in Fig. 4 for different numbers of Cu ML. Also shown in Fig. 4 as an intensity contour plot are the new experimental PE QWS energies (at the intensity maxima). The calculated QWS energies fall within about 0.1 eV of the experimental values, and the agreement improves with increasing Cu thickness. Interestingly, our calculated QWS energies agree well with previously calculated results by Van Gelderen *et al.*,[12] although their LDA Δ_1 band dispersion differs from ours. However, our band structure corrected calculations provide *sp*-like QWS in an energy window of E-E$_F$ from 0 to

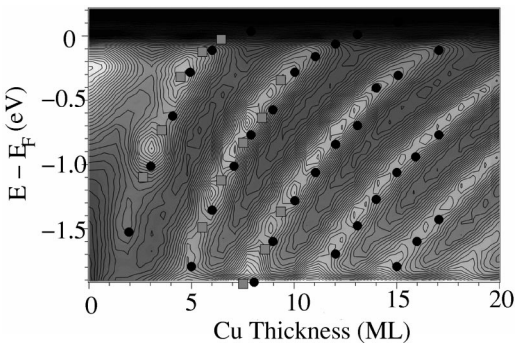

FIG. 4. The experimental photoemission yield is shown in contour as a function of Cu ML along with the QWS energies calculated using the corrected Cu bands and GGA (denoted with filled circles). QWSs for interdiffusion interface layers of Co and Cu are depicted with gray squares.

-2.0 eV in agreement with the experiments. In contrast, previous uncorrected LDA calculations showed a dense pattern of *d*-like QWS around -1.6 eV down to -2.0 eV.

In Fig. 4, one can draw a horizontal line for a given energy E. The oscillation periodicity of the PE intensity along this line is a manifestation of the crystal momentum wave number $k_\perp$ for this given energy. For example, our calculated oscillation period of the QWS at the Fermi energy E_F is 5.7 ML, which is in good agreement with our experimental value of 5.6 ML. This corresponds to Fermi wave numbers of $k_F = 1.435$ and 1.429 Å^{-1}, respectively, for the calculated and experimental results. Both numbers correspond well with known de Haas–van Alphen data: $k_F/k_{BZ}=0.827$ ($k_F = 1.439$ Å^{-1}), where k_{BZ} is the Brillouin zone boundary.[28]

C. Phase accumulation model

The phase accumulation model (PAM) (Refs. 15,29, and 30) is often used to describe the quantization of QWSs. Conceptually, it envisions a plane wave propagating inside the quantum well. As the plane wave reaches the surface (or interface) of the thin film, it will be reflected back with an additional surface (interface) phase θ_S (θ_I). After the plane wave has been reflected at both surfaces, it can undergo constructive or destructive interference with itself. For constructive interference the total accumulated phase must be an integer multiple of 2π. Thus, the quantization condition for the existence of a QWS is given by

$$2k_{eff}d-\theta_I-\theta_S=2\pi\nu,$$

$$2k_\perp d+\theta_I+\theta_S=2\pi(N-\nu), \tag{1}$$

where $k_\perp=k_{BZ}-k_{eff}$ is the crystal momentum wave vector perpendicular to the film surface, $k_{BZ}=\pi N/d=2\pi/a$, d is the Cu thickness (the number of Cu ML, N, times the interlayer spacing, $a/2$), and θ_S and θ_I are electron-wave reflection phases at the Co/Cu and the Cu/vacuum interfaces, respectively. Notice that in Eq. (1), $k_\perp$ is a function of plane wave energy E. In order to determine QWS energies using Eq. (1), one also needs to know θ_S and θ_I as functions of the plane wave energy E. In the PAM model, these are provided by the following phase formulas[15]:

$$\theta_S=\pi\sqrt{\frac{3.4(eV)}{E_V-E}}-\pi, \tag{2}$$

$$\theta_I=2sin^{-1}\sqrt{\frac{E-E_L}{E_U-E_L}}-\pi, \tag{3}$$

where in this case $E_V=4.4$ eV, $E_L=-3.9$ eV, $E_U=-0.58$ eV, and E is evaluated with respect to the Fermi energy E_F. Equation (2) has been derived with the hydrogenic description of the surface potential barrier with a classical image charge in the WKB approximation, and Eq. (3) is derived from a semiempirical expression[29,30] based on the $sp-d$ band hybridization gap of Co. In an application of the PAM model, the $k_\perp(E)$ curve is approximated by the nearly free electron dispersion which describes very well the *sp*-like Δ_1 band near the Fermi level. Thus, the main source of error in the PAM comes from the phases described in Eqs. (2) and (3).

In order to analyze the deficiencies in the PAM description of phases, we adopt two different but complementary approaches to evaluating the phases and the surface-normal wave numbers $k_\perp$ in our computed QWSs. First, we apply Eq. (1) to Fig. 4. In Fig. 4, if we draw one horizontal line, then $k_\perp$, θ_S, θ_I will be the same along this line. What is changing along this line is the d and ν in Eq. (1). From one peak of PE intensity to another peak, ν increases by 1 while d increases by some amount Δd. Thus we obtain $k_\perp=k_{BZ}-(1/2)(2\pi/\Delta d)$ from Eq. (1), independent of the phase value of θ_S and θ_I. After $k_\perp$ is obtained, the total phase $\theta_T=\theta_I+\theta_S$ can be calculated at the first peak from the left in Fig. 4, assuming $\nu=1$ and using Eq. (1). For the experimental data, in order to determine the PE intensity peak positions more accurately, we have fitted the PE intensity curve with a sinusoidal function $I(d)=a+b\cos(2k_{eff}d-\theta_T)$ for each given energy E. This is essentially the same procedure as we discussed above. The $k_\perp(E)$ curve obtained this way from our calculated data in Fig. 4 reproduces almost exactly our bulk band structure results of the *sp*-like Δ_1 band shown by the solid curves in Fig. 2. However, the $k_\perp(E)$ obtained from the experimental data in Fig. 4 deviates slightly from our theoretical results. This is shown as the dashed curves in the inset of Fig. 2. Since our LDA-corrected theoretical band structure is fitted to experimental bulk Cu photoemission data, this means that the experimental curve $k_\perp(E)$ from the current thin film experiment might be slightly different from the direct bulk Cu photoemission experimental results.

The second approach to analyzing the theoretical results is a more sophisticated fitting procedure. In this procedure, two Bloch waves running in opposite directions with wave vectors $k_\perp$ and $-k_\perp$ are used to construct the calculated quantum well state away from the interface and surface. More precisely, we have

$$\psi_{Fit}(\mathbf{r})=u_{\mathbf{k}}(\mathbf{r})e^{ik_\perp z}+u^*_{\mathbf{k}}(\mathbf{r})e^{-i(k_\perp z+\theta)}, \tag{4}$$

where $u_{\mathbf{k}}(\mathbf{r})$ is the periodic part of the Bloch wavefunction obtained in a bulk Cu calculation. $\psi_{Fit}(\mathbf{r})$ is used to fit the calculated quantum well state $\psi_{QW}(\mathbf{r})$. More precisely, we maximized the overlap $F=|\int_{z1}^{z2}\psi^*_{QW}(\mathbf{r})\psi_{Fit}(\mathbf{r})d^3r|^2/\int_{z1}^{z2}|\psi_{Fit}(\mathbf{r})|^2d^3r$, by sweeping through $k_\perp$ and θ, where $z1$, $z2$ delimit the fitting region as indicated in Fig. 3. The fitted $k_\perp$ agrees with the result calculated from the data in Fig. 4, and the calculated bulk band structure shown in Fig. 2. This microscopic fitting procedure provides a $\sim$99% overlap for a fitting region starting one atom above the interface Cu and ending one atom below the surface Cu for Co_4/Cu_n thin films. Two fitted $\psi_{Fit}(r)$ wavefunctions squared are shown as dashed lines in Fig. 3 for $\nu=2$ and 3. In the fitting region, there is almost no difference between the directly calculated and the fitted wavefunctions. The only significant difference appears outside the last layer of Cu atoms, as expected. This confirms that the phase accumulation model concept of two

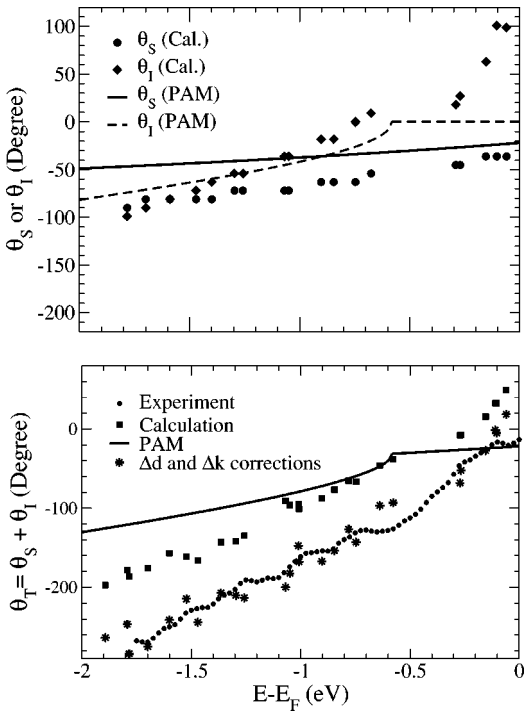

FIG. 5. The top panel shows the interface and surface reflection phases θ_I and θ_S determined by our fitting method and also given by the PAM expressions for the phases in Eqs. (2) and (3). The bottom panel indicates the total phases $\theta_T=\theta_I+\theta_S$, given by the PAM, our fitting method, the experiment and our correction.

oppositely running Bloch wave functions is sufficient to model the QWSs in the quantum well region. Notice that this assumption is not automatic: there could be other bulk wave functions in the construction of the QWSs; and near the surface, there could be evanescent states from other bands which have the same energy but an imaginary $k_\perp$. Our calculation shows that these evanescent states decay almost to zero as soon as we are inside the Cu layers.

The total phases θ_T fitted using Eq. (1) from the experimental data and theoretical data in Fig. 4 are shown as solid circles and squares in the bottom panel of Fig. 5. Also shown as the solid curve in the bottom panel of Fig. 5 is the total phase of the PAM model according to Eqs. (2) and (3). There are large differences between these three sets of results. In our microscopic fitting of Eq. (4), besides the total phase $\theta_I+\theta_S$, we can also obtain the individual phases θ_I and θ_S. By definition, θ_S (θ_I) is the phase θ ($-\theta$) when the zero of z in Eq. (4) is defined at z_S (z_I), the reflection point of the Cu surface (interface). Here we define z_S and z_I to be one-half of a monolayer beyond the last Cu nuclei of the surface and interface, respectively. This definition is consistent with the definition of the total thickness of Cu layers in Eq. (1). The fitted θ_I and θ_S determined this way are shown in the top panel of Fig. 5. They are both different from the PAM formula results. Note that the sum of the microscopically fitted θ_I and θ_S almost exactly equals the total phase fitted from the theoretical data points in Fig. 4 using Eq. (1).

The calculated reflection phases θ_I, θ_S at the Co/Cu and Cu/vacuum interfaces deviate significantly from the PAM phases, and the calculated total phases θ_T lie between the PAM results and our experimental results. The calculated total phase differs from experimental results by about 60°–80°, while the simple PAM formula differs from experiment by about 100°–150°. In addition, the PAM phase at the interface, θ_I, is set equal to zero for $E\text{-}E_F > -0.58$ eV when resonance coupling appears between the *sp*-like states in Co layers and Cu layers. Thus, we find on the one hand that the PAM model provides an excellent qualitative picture and that Eq. (1) is valid conceptually, and, on the other hand, that the current formulas for the PAM phases [Eqs. (2) and (3)] need to be modified to get quantitatively accurate results. It is worth mentioning that the uncertainty at the starting point of the Cu wedge can give a correction of $\Delta\theta_T=2k_{eff}\Delta d$ to the PAM phase. We have found that the correction improves the QWS fitting in the energy-thickness plane, but can never bring the PAM phase in agreement with the experimental phase.

To shed some light on the deviation of our calculated total phase from experiment, let us consider the effect of the small $k_\perp(E)$ difference $\Delta k_\perp = k_{BZ} - \Delta k_{eff}$ between the theoretical/bulk PE experimental result and the current thin film fitted experimental result, and of the possibility of some uncertainty in the position of the Cu surface. We will use an uncertainty Δd of the total thin film thickness to describe this uncertainty at the surface. To this end, we can express the resulting change in the theoretical total phase $\Delta\theta_T$ as

$$\Delta\theta_T = 2k_{eff}(E)\Delta d + 2\Delta k_{eff}(E)d. \tag{5}$$

Since Δk_{eff} is fixed in our calculation, the only free parameter is Δd. To bring our theoretical result close to the experimental result θ_T, we have found that Δd would need to be -0.9 Å, which corresponds to half a monolayer. The reduction of Cu thickness by 0.5 ML alone already leads to fairly good agreement with the experiment. After this $\Delta\theta_T$ of Eq. (5), the calculated total phase is in agreement with the experimental results, as shown in Fig. 5.

D. Surface potential correction in the LDA calculation

The above analysis of $\Delta\theta_T$ is illuminating. It shows that the difference between the calculated total phase and the experimental one can be explained by some correction to the surface. This is also consistent with the comparison in Fig. 4. The difference between the calculated QWS energy and the experimental one is about 0.1 eV for small d, while it decreases significantly for larger d. One possible surface correction to the LDA calculation is the surface image potential. It is well known that the LDA calculation fails to reproduce the $-e/4z$ image potential that exists near a metal surface.[31–35] Quantum mechanically, this image potential is due to the exchange-correlation hole. At the surface, this exchange-correlation hole at a given point r becomes highly nonlocal and asymmetric around r. Essentially, even if r is away from the surface, this exchange-correlation hole cannot leave the metal and thus forms an image charge at r, which gives rise to the image potential. Unfortunately in a LDA

calculation, the approximated exchange-correlation hole always surrounds r with a spherical symmetry. Many researchers have studied this problem using different methods: the external potential perturbation method,[31] weighted density approximation,[32,33] and the *GW* method.[34,35] The correction to the LDA image potential is negative away from the surface, which would lower the calculated QWS energies, bringing them even further from the experimental values (see Fig. 4). However, in all the beyond-LDA calculations of the image potential,[32–35] while there is a negative -e/4z additional potential to the LDA away from the surface, there is always a small positive correction near the surface.

The QWSs are strongly peaked near the surface since they have antinodes at the surface; therefore a small change in the potential there will significantly change their energies. We have taken the correction to the LDA potential Δv from Ref. 33, and performed a zero-order estimation based on $\int \Delta v(r)|\psi(r)|^2 d^3r$ for the change in the quantum well eigenstate energy. We found that the eigenstate energy can be easily shifted upward by more than 30 meV for small copper thicknesses, bringing it closer to the experimental value. Even higher shifting is possible, depending on the model and parameters used. The correction will be less significant as the number of layers of copper increases and surface effects become relatively less important. This can explain why the error between theory and experiment decreases with increasing copper thickness. However, since different methods[31–35] tend to give different Δv near the surface, we feel that a more quantitative treatment is not warranted at this point. Nevertheless, the error in the LDA surface potential could be a reason for the discrepancy between theory and experiment that we see in Figs. 4 and 5.

E. Effect of interdiffusion on QWSs

We have also investigated theoretically the influence on quantum well states of a possible interdiffusion at the Co/Cu interface, which could take many forms. Such an interface was modeled very roughly and simply to obtain a qualitative picture, by replacing the perfect Cu layer at the Co/Cu interface with a 50:50 mixed layer of Co and Cu, arranged in a checkerboard pattern of a doubled supercell. This model corresponds to shifting the average interface halfway between the integer-monolayer values discussed so far. One may expect the resulting QWS energies to fall between those for perfectly sharp interfaces; however, the exact values will depend on details of the wave functions and reflection phases, and thus need not be simple averages of those for perfect interfaces. The calculated resulting QWS energies indeed fall on the dominant QWS curves as denoted with filled squares in Fig. 4, thus interpolating between the energies for integer-monolayer films. This suggests that the QWSs have a tolerance to interdiffusion across the interface. It also shows that interdiffusion can contribute to the ''smearing'' of the curves seen in Fig. 4, which reduces the resolution of individual peaks at integer Cu thicknesses. For instance, for $Co_{4.5}/Cu_{2.5}$ with a 50:50 mixed interface layer, a QWS level resides at $E\text{-}E_F = -1.13$ eV that falls on an interpolation curve for $\nu = 1$ between the results for Co_4/Cu_2 and Co_4/Cu_3. Similarly, $Co_{4.5}/Cu_{5.5}$ has two QWSs at $E\text{-}E_F = -1.48$ eV and -0.15 eV that fall on the interpolation curves for $\nu = 2$ and 1 in Fig. 4, respectively.

Another interesting aspect of the interdiffusion is connected to the foregoing phase correction of $\Delta d = 0.9$ Å in Eq. (5). According to our calculation, a Co_{4+x}/Cu_{n-x} film has an effective thickness of $d = (n-x)*a/2$. This opens up the possibility of fractional-monolayer thicknesses. It poses a difficult task for experimental determination of d. Currently, zero d is assigned in our wedge experiment by finding individual spots in the PE intensity in Fig. 4, and assuming that these spots correspond to integer numbers of monolayer thickness. Further investigation is needed to clarify this point.

V. CONCLUSIONS

We have measured new photoemission intensity data of unprecedented accuracy that allow for the close examination of phases and nodal structures of QWSs in the Co/Cu_n systems. Up until recently, the combined method of the nearly free electron model and the PAM model has been used primarily to fit the QWS energy as a function of Cu thickness in the Co/Cu_n systems. However, our photoemission data and calculations indicate that the PAM model, while correct in concept, is not accurate with the simple assumed PAM phase expressions that are commonly used with it. On the other hand, if one uses the experimental phases (derived from a plot like that of Fig. 4), the PAM method provides an accurate description of the QWS energy as a function of Cu thickness.

Our calculations with the corrected Cu band structure have shown that the calculated QWS energies fall within about 0.1 eV of the experimental values, improving LDA results which give errors of about 0.3 eV with respect to the experiment. The QWS oscillation periodicities evaluated from the calculated energy-thickness relation ($E(d)$) prove to be consistent with the corrected Cu band structure but differing slightly from the fitted band of the experimental QWS (see Fig. 2). The *sp*-like QWSs have been accurately calculated down to $E\text{-}E_F = -2.0$ eV; we therefore do not observe the dense set of QWS arising from the Cu *d*-like Δ_5 band seen in that range in the calculations of Nordström *et al.*[10]

To verify the validity of the PAM model, we have constructed a standing wave as a superposition of two bulk Bloch waves running in opposite directions, and the resulting standing wave describes the full QWS wave functions with an accuracy of 99% within the film. This confirms that the PAM concept of two oppositely running wavefunctions is sufficient to accurately model the QWS if those wavefunctions are chosen to be accurate bulk eigenstates.

We have obtained surface and interface reflection phases in different ways, both from experiment and theory. The difference of phases between theory and experiment can be qualitatively explained as due to an inadequacy of the LDA/GGA description of the image potential. By taking into account an additional positive potential near the surface, based on earlier models, the calculated QWS energy eigenvalues

and phases shift nearer to experiment; this results from an electron wave function peak near the surface. In other words, the additional positive potential near the surface reduces the effective width of the potential well.

Our simple model of interdiffusion at the Co/Cu interface suggests that the QWSs have a tolerance to such interdiffusion: the QWS energies remain close to the dominant E vs *d* curves visible in Fig. 4, thus approximately interpolating between QWS energies for neighboring integer-monolayer film thicknesses. Such interdiffusion thus would smear out the dominant curves (ridges) in Fig. 4, reducing the sharpness of the peaks seen in those curves.

ACKNOWLEDGMENTS

The theoretical work was supported in part by the Laboratory Directed Research and Development Program of Lawrence Berkeley National Laboratory under the Department of Energy Contract No. DE-AC03-76SF00098. This experimental work was funded in part by National Science Foundation under Contract No. DMR-0110034, and by the U.S. Department of Energy under Contract No. DE-AC03-76SF00098. This research used resources of the National Energy Research Scientific Computing Center and the Advanced Light Source, which are supported by the Office of Science of the U.S. Department of Energy.

*Electronic address: jman@lbl.gov

[1] S.S.P. Parkin, N. More, and K.P. Roche, Phys. Rev. Lett. **64**, 2304 (1990).
[2] J.E. Ortega and F.J. Himpsel, Phys. Rev. Lett. **69**, 844 (1992).
[3] R.K. Kawakami, E. Rotenberg, H.J. Choi, J.H. Wolfe, N.V. Smith, and Z.Q. Qiu, Phys. Rev. Lett. **82**, 4098 (1999).
[4] W. Weber, A. Bischof, R. Allenspach, C. Würsch, C.H. Back, and D. Pescia, Phys. Rev. Lett. **76**, 3424 (1996).
[5] D.A. Luh, T. Miller, J.J. Paggel, M.Y. Chou, and T.C. Chian, Science **292**, 1131 (2001).
[6] V.N. Strocov *et al.*, Phys. Rev. Lett. **81**, 4943 (1998).
[7] V.N. Strocov *et al.*, Phys. Rev. B **63**, 205108 (2001).
[8] A. Marini, G. Onida, and R.D. Sole, Phys. Rev. Lett. **88**, 016403 (2002).
[9] V.N. Strocov, R. Claessen, P.B.F. Aryasetiawan, and P.O. Nilsson cond-mat/0211228 (unpublished).
[10] L. Nordström, P. Lang, R. Zeller, and P.H. Dederichs, Europhys. Lett. **29**, 395 (1995).
[11] L. Nordström, P. Lang, R. Zeller, and P.H. Dederichs, J. Appl. Phys. **79**, 8 (1996).
[12] P. van Gelderen, S. Crampin, and J.E. Inglesfield, Phys. Rev. B **53**, 9115 (1996).
[13] W. Kohn and L.J. Sham, Phys. Rev. **140**, A1133 (1965).
[14] U. von Barth and L. Hedin, J. Phys. C **5**, 1629 (1972).
[15] N.V. Smith, N.B. Brookes, Y. Chang, and P.D. Johnson, Phys. Rev. B **49**, 332 (1994).
[16] R.K. Kawakami, M.O. Bowen, H.J. Choi, E.J. Escorcia-Aparicio, and Z.Q. Qiu, Phys. Rev. B **58**, 5924 (1998).
[17] P. Hohenberg and W. Kohn, Phys. Rev. **136**, B864 (1964).
[18] J.P. Perdew, J.A. Chevary, S.H. Vosko, K.A. Jackson, M.R. Pederson, D.J. Singh, and C. Fiolhais, Phys. Rev. B **46**, 6671 (1992).
[19] J.P. Perdew, K. Burke, and M. Ernzerhof, Phys. Rev. Lett. **77**, 3865 (1996).
[20] The plane-wave pseudopotential code PETOT was originally developed by L. W. Wang while at the National Renewable Energy Laboratory; PARATEC (Parallel Total Energy Code) by B. Pfrommer, D. Raczkowski, A. Canning, and S. G. Louie, Lawrence Berkeley National Laboratory with contributions from F. Mauri, M. Cote, Y. Yoon, C. Pickard, and P. Haynes.
[21] M. Fuchs and M. Scheffler, Comput. Phys. Commun. **119**, 67 (1999).
[22] D.R. Hamann, Phys. Rev. B **40**, 2980 (1989).
[23] N. Troullier and J.L. Martins, Phys. Rev. B **43**, 1993 (1993).
[24] N. Marzari, D. Vanderbilt, A.D. Vita, and M.C. Payne, Phys. Rev. Lett. **82**, 3296 (1999).
[25] B.G. Pfrommer, M. Coté, S.G. Louie, and M.L. Cohen, J. Comput. Phys. **131**, 233 (1997).
[26] A. Marini, G. Onida, and R.D. Sole, Phys. Rev. B **64**, 195125 (2001).
[27] L.W. Wang, Appl. Phys. Lett. **78**, 1565 (2001).
[28] P.T. Coleridge and I.M. Templeton, Phys. Rev. B **25**, 7818 (1982).
[29] E.G. McRae and M.L. Kane, Surf. Sci. **108**, 435 (1981).
[30] P.M. Echenique and J.B. Pendry, Prog. Surf. Sci. **32**, 111 (1989).
[31] N.D. Lang and W. Kohn, Phys. Rev. B **1**, 4555 (1970).
[32] P. Garcia-Gonzalez, J. Alvarellos, E. Chacon, and P. Tarazona, Phys. Rev. B **62**, 16063 (2000).
[33] S. Ossicini and C. Bertoni, J. Vac. Sci. Technol. A **5**, 727 (1987).
[34] A.G. Eguiluz, M. Heinrichsmeier, A. Fleszar, and W. Hanke, Phys. Rev. Lett. **68**, 1359 (1992).
[35] J.J. Deisz and W.H.A.G. Eguiluz, Phys. Rev. Lett. **71**, 2793 (1993).